

Highlights

First-Principle Analysis of Hydrogen Storage Potentials in Vanadium Hydride Perovskites XVH_3 ($X = Li, K$)

Anupam, Shyam Lal Gupta, Sumit Kumar, Ashwani Kumar, Sanjay Panwar, Diwaker

- Stability of XVH_3 ($X = Li, K$) hydride perovskites is confirmed by Enthalpy of formation.
- The gravimetric hydrogen storage capacity for XVH_3 ($X = Li, K$) are 3.25% and 4.97%
- Metallic behavior is revealed by electronic structure of these hydrides.
- Enhanced potential for alternative green energy source.

First-Principle Analysis of Hydrogen Storage Potentials in Vanadium Hydride Perovskites XVH_3 ($X = Li, K$)

Anupam^a, Shyam Lal Gupta^b, Sumit Kumar^c, Ashwani Kumar^d, Sanjay Panwar^{a,*} and Diwaker^{e,**}

^aSchool of Basic and Applied Sciences, Maharaja Agrasen University, Baddi, Solan, 174103, H P, INDIA

^bDepartment of Physics, HarishChandra Research Institute, Prayagraj, Allahabad, 211019, U P, INDIA

^cDepartment of Physics, Government College, Una, 174303, H P, INDIA

^dDepartment of Physics, Abhilashi University, Mandi, 175045, H P, INDIA

^eDepartment of Physics, SCVB Government College, Palampur, Kangra, 176061, H P, INDIA

ARTICLE INFO

Keywords:

Hydrogen Storage

Perovskites

Li and K metal-Hydrides

Gravimetric hydrogen storage capacity

Desorption temperature

ABSTRACT

This study investigates Vanadium-based XVH_3 ($X = Li, K$) hydride perovskites for their hydrogen storage capacity using the WIEN2K code. Structural studies reveal that these hydrides are stable and belongs to cubic space group (221 Pm-3m). We have examined many aspects of these compositions throughout, using the PBE-GGA and mBJ exchange correlation potential. The study also examines their thermodynamic stability and gravimetric hydrogen storage capacity. The findings suggest metallic nature of these compositions and strong thermoelectric responses, making them potential candidate for green energy sources.

1. Introduction

Perovskites with exceptional qualities have become one of the most fascinating new materials for the twenty-first century. Perovskite has attracted a lot of attention and made substantial strides in energy storage, pollutant degradation, and optoelectronic devices in the last several decades because to its remarkable photoelectric and catalytic properties[1]. Materials of the empirical formula ABX_3 are referred to as perovskites. These materials are further divided into two groups: organic-inorganic hybrid perovskite and inorganic perovskite. $SrTiO_3$ is a prime example of a perovskite due to its unique structure in the lower symmetric space group. The recent studies on various transition metal hydrides, complex hydrides and carbon based compounds can be act as better alternative for green energy demand globally [2, 3, 4, 5, 6, 7, 8, 9, 10, 11, 12, 13, 14, 15]. Perovskite, with its characteristic magnetic and electric properties, holds potential for developing novel hydrogen storage applications due to its affordable cost and fascinating physical and chemical features. Alkali and alkaline earth metals, A and B, respectively, make up perovskites hydrides, which are ionic compounds with predicted band gaps of at least 2 eV. The stability trend of tolerance factors largely supports Goldschmidt's theory. The chemical compound known as perovskite hydrides, or ABX_3 , has drawn interest lately as a potential viable hydrogen storage solution. Although perovskite materials have significant role in storing Hydrogen but no such significant compounds found in study or literature yet. So the materials which met the Hydrogen storing requirements are still being continuously searched [16, 17, 18, 19, 20, 21, 22, 23, 24, 25,

26, 27, 28, 29, 30]. Materials for storing hydrogen often have lot of hydrogen bonding in these materials. They have four key characteristics: (1) they are large enough to hold large amounts of hydrogen; (2) they possess catalytic qualities that improve hydrogen absorption; and (3) they have adequate gravimetric hydrogen storage capacities that improve hydrogen storage. The gravimetric densities of hydroxide perovskites typically range from 1.2 to 6.0 weight percent. Hydrogen may be stored more effectively and safely in metal hydride perovskites than in liquid or compressed gas phase [31, 32, 33, 34, 35, 36]. This study explores the structural, electronic, thermodynamic, thermoelectric, mechanical, and hydrogen storage characteristics of perovskite hydrides with a specific pairing XVH_3 ($X = Li, K$) for hydrogen storage applications using density functional theory.

2. Computational details

The XVH_3 ($X = Li, K$) cubic phase structure is taken into consideration for all compositions by using space group 221 (Pm-3m) to investigate different properties using WIEN2k [37, 38]. The structural properties were calculated using Perdew Burke Ernzerhof (PBE) and the generalized gradient approximation (GGA) while the electronic behaviour is explored using mBJ functional. This is because modified Becke-Johnson (mBJ) functional is reported to predict reliable band structure [39] even more correctly and fast compared to the usual hybrid functional approach [40, 41, 42] in Wien2K. Birch-Murnaghan's equation of state [43, 44, 45, 46] is used to explore the structural characteristics and determine the stable phase of these perovskites. All these calculations uses 216 k-points, an RMT of 5.0, and an energy cutoff of -6.0 Ryd. Geometrically optimized calculations were used to compute the structural, electronic, thermodynamic, thermoelectric, mechanical, and hydrogen storage properties of cubic compositions XVH_3 ($X = Li, K$).The WIEN2k code has been used for all calculations.

*Corresponding author

**Principal corresponding author

 dr.spanwar@gmail.com (S. Panwar); diwakerphysics@gmail.com (

Diwaker)

ORCID(s): 0000-0003-3283-3165 (S. Panwar); 0000-0002-4155-7417 (Diwaker)

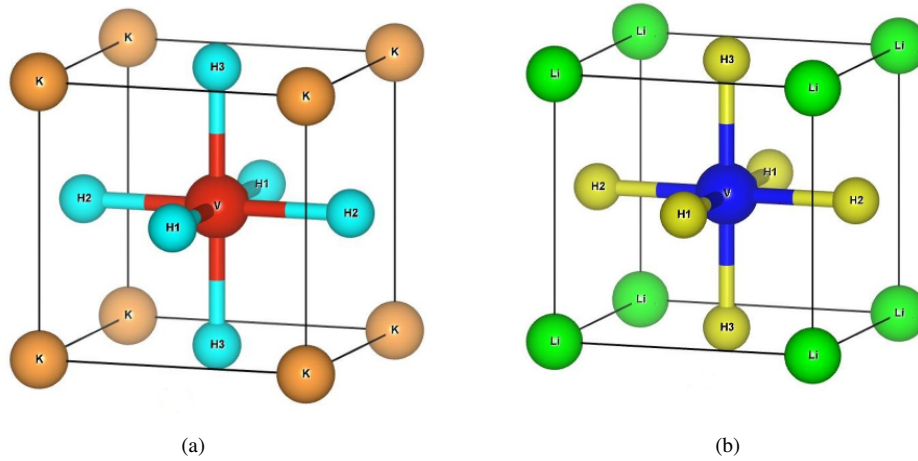


Figure 1: Optimised crystal structure of (a) KVH₃ (b) LiVH₃

Table 1

Lattice constants [*a* (Å)], Bulk Modulus (*B* in GPa), Volume (*V*₀ in Å³), Pressure derivative of Bulk modulus (*B*' in GPa), Ground state Energy (*E*₀ (eV)), enthalpy of formation (ΔH_f (KJ/mol.H₂)), decomposition temperature (*T*_d) and Gravimetric storage densities (*C*_{wr%}) of XVH₃ with (X=Li, K) perovskites.

Perovskite	<i>a</i>	<i>B</i>	<i>V</i> ₀	<i>B</i> '	<i>E</i> ₀	ΔH_f	<i>T</i> _d	<i>C</i> _{wr%}
KVH ₃	3.8341	56.99	380.36	3.97	-3106.31	-457.27	3499	3.25
LiVH ₃	3.4505	80.15	277.21	4.62	-1917.18	-248.86	1904	4.97

Thermal investigations has been done using BoltzTrap2 code[47] while Gibbs 2 code[48] is used for thermodynamic investigations.

3. Results and Discussions

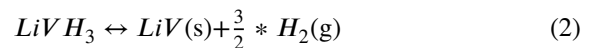
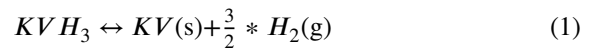
This section will explore the structural, electronic, thermodynamic, thermoelectric, mechanical, and hydrogen storage properties of vanadium-based XVH₃ hydride perovskites.

3.1. Investigations of Structural Phase Stability on XVH₃ (X = Li, K)

The proposed hydride perovskites adopt FCC symmetry with space group 221(Pm-3m), with a general formula ABH₃, where A is a cation usually Alkali metals (Li and K in our case) while B is a transition metal (V in our case) which forms a octahedral coordination with different hydrogen atoms. The Wyckoff positions of A species (Li and K in our case) occupy Wyckoff positions 1a (0,0,0) and B species which is V in our case is placed at Wyckoff positions 1b (0.5,0.5,0.5) while the three hydrogens are at Wyckoff positions 3c as (0, 0.5, 0.5), (0.5, 0, 0.5), and (0.5, 0.5, 0), respectively. Figure 1 shows the relaxed crystal structure of XVH₃ (X = Li, K) hydrides perovskites. Figure 2 (a-b) displays energy vs volume graphs that illustrate the minimal ground state energy of these compositions. Table 1 lists parameters like Lattice constants, Bulk Modulus, Volume, Pressure derivative, Ground state Energy, enthalpy of formation, decomposition temperature, and Gravimetric storage densities of XVH₃ (X= Li, K) perovskites.

3.2. Stability, enthalpy, decomposition temperature and hydrogen storage of the inter-metallic hydrides

The stability of intermetallic hydrides has been predicted using the enthalpy of production (ΔH_f) and the decomposition temperature (*T*_d). Phase stability and dehydrogenation properties are found for XVH₃ (X = Li, K) hydrides perovskites. The reactions that result in XVH₃ (X = Li, K) perovskites may be comprehended using the following equations.



Using Hess law as given below

$$\Delta H_f = \sum E_{tot}(\text{products}) - \sum E_{tot}(\text{reactants}) \quad (3)$$

The enthalpy of formation for these compositions with (X=Li,K) is calculated using the equation given below

$$\Delta H_f = E_{tot}(XVH_3) - E_{tot}(XV) - \frac{3}{2} E_{tot}(H_2) \quad (4)$$

Notably, we get a formation enthalpy of -457.27kJ/mol.H₂ and -248.86 kJ/mol.H₂ using the FP-LAPW technique for (X=K, Li) proving these perovskites' exceptional thermodynamic stable. Further, the standard Gibb's energy (ΔG) relation is given as

$$\Delta G = \Delta H_f - T\Delta S \quad (5)$$

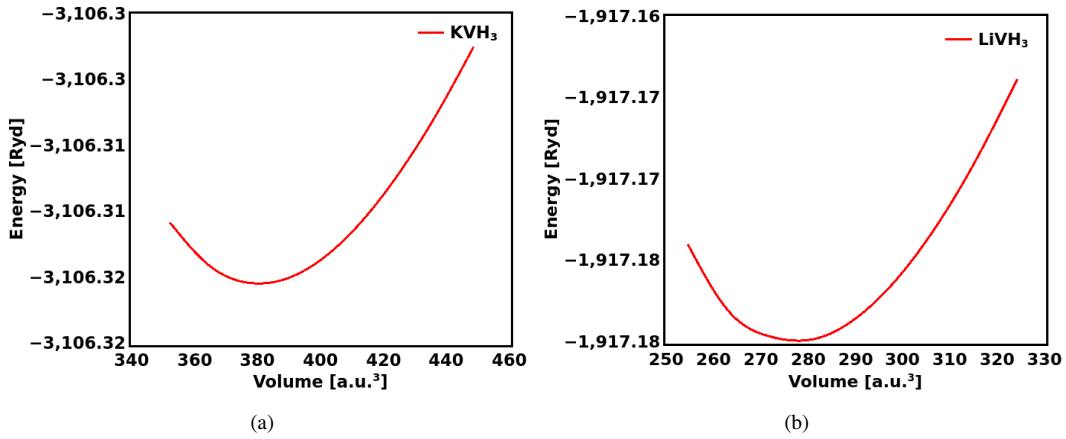


Figure 2: Energy versus Volume curves of (a) KVH₃ (b) LiVH₃

where ΔH_f is formation enthalpy and ΔS is standard entropy change for hydrogen. At equilibrium, the standard value of Gibb's energy is zero. Further, if we talk about the value of change in entropy i.e ΔS it results from the way the hydrogen molecule changes during the dehydrogenation reaction as $\Delta S = 130.68 J/mol.K^{-1}$ [49]. Therefore, the thermal decomposition T_d [49] can be calculated using the relation given as

$$T_d = -\frac{\Delta H_f(inJ/mol)}{130.68} \quad (6)$$

The calculated decomposition temperature for KVH₃ was 3499 K and for LiVH₃ was 1904 K using the enthalpy of formation value from Table 1 in the aforementioned equation. These indicate the potential of studied compositions for high temperature hydrogen cyclability. Understanding the gravimetric hydrogen storage capacity of these compositions is crucial for their application in hydrogen storage applications. The term "gravimetric hydrogen storage capacity" refers to the amount of hydrogen that may be stored per mass unit of a substance. Using the equation below, the gravimetric hydrogen storage capacities $C_{wt\%}$ [50] for the compositions under study are determined.

$$C_{wt\%} = \left[\frac{n_H * M_H}{M_{(XVH_3)}} \times 100 \right] \% \quad (7)$$

In this case, the number of hydrogen atoms is n_H , the molar mass of hydrogen is M_H , and the molar mass of the compound is $M_{(XVH_3)}$. From the above formula after calculation, the gravimetric hydrogen storage capacity is found to be 3.25% and 4.97% for XVH₃ (X=Li, K) respectively. These are close to the DOE set targets of 5.5 % till end of 2025 for light duty fuel cell vehicles as reported by US Department of energy. The authors have investigated one formula unit of our compositions which shows these gravimetric hydrogen capacity but if we consider thin films of these materials they have enhanced gravimetric hydrogen capacity [31, 33, 32].

3.3. Energy band topologies, density of state plots

The amazing electronic properties of perovskites, a class of materials with a distinctive crystal structure, have garnered a lot of interest lately. Perovskite materials, due to their tunable bandgap, are versatile and can be utilized in various applications such as photodetectors, solar cells, LEDs, and hydrogen storage. Along the high symmetry sites in the first Brillouin zone, the energy band structure for XVH₃ (X = K, Li) hydride perovskites is computed and displayed in figures 3(a-b). In order to compare the strength of the electronic correlations among different species in a particular composition, we also calculated the band structure using PBE-GGA and compared with those obtained from mBJ approach (See appendix 1). It can be seen from figures as reported in appendix 1 that both approaches lead to the same band structure. This indicates that these are weakly correlated systems. D.O.S. is a fundamental concept in solid-state physics, indicating the density of electronic states in a material at a specific energy level. DFT investigation reveals metallic compounds with no energy gap between valence and conduction bands. Total (T.D.O.S.) and partial density of states (P.D.O.S.) of XVH₃ were calculated for electronic contribution. Figure 4 (a-c) shows the plots T.D.O.S. and P.D.O.S. of XVH₃ (X = K, Li) hydride perovskites. For KVH₃ and LiVH₃, the greatest value of T.D.O.S. in the valence band is 0.9 states/eV and 0.75 states/eV, respectively. The understanding of the electronic structure of materials can be facilitated by the partial density of states. It offers details on the density of states of a particular element or material's orbital. We note that a significant contribution has come from the d-states in KVH₃ and p states in LiVH₃. This can be attributed to different electropositivity of different alkali metals present in these compositions.

3.4. Lattice dynamic stability

The dynamical stability of metal hydride XVH₃ with (X=Li, K) has been determined via phonon dispersions in the Brillouin zone as represented in Figure. 5(a-b). The optical behaviour of hydride materials is caused by the optical branches, which are found in the top region of the dispersion

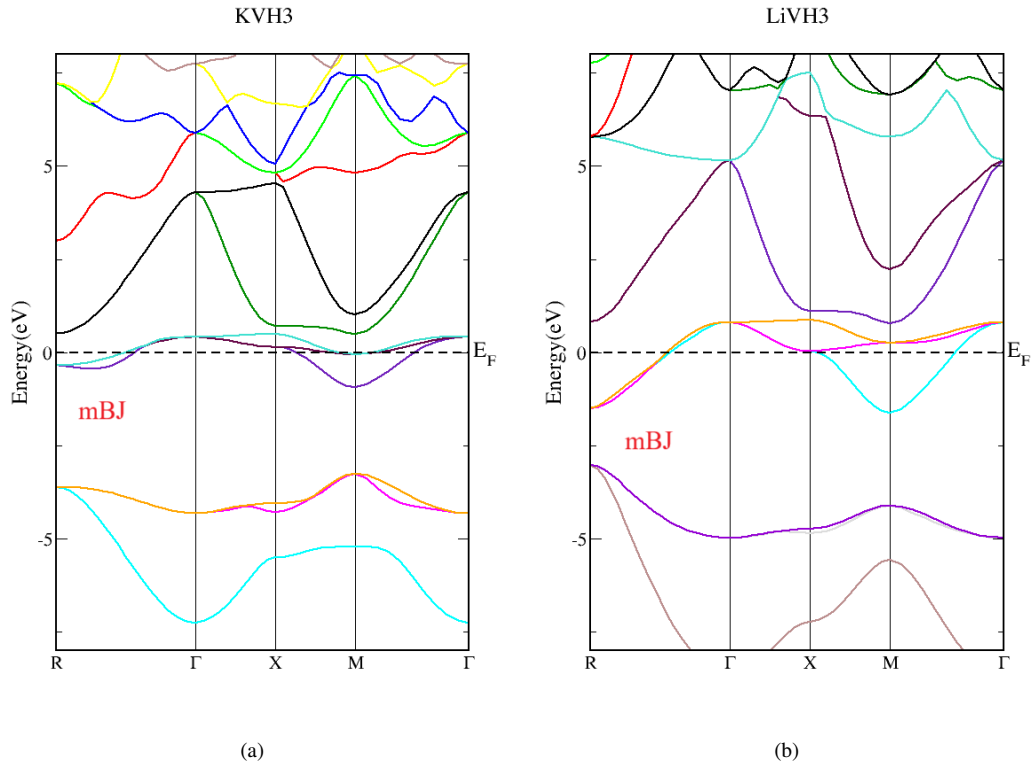


Figure 3: Energy Band structures using mBJ approach [a] KVH₃ [b] LiVH₃

curves. These optical modes are the result of atoms in a lattice oscillating out of phase. Conversely, acoustic branches, which are located at the bottom of phonon dispersion curves, originate from the coordinated vibration of atoms in a lattice beyond their balance position. According to literature stable structure only contains positive vibration states within phonon dispersion curves. The crystal bonding energy will be lost in the negative vibration states, and occasionally the structure will vanish as a result of breaking of atomic bonds. Therefore, the absence of negative frequencies throughout the whole Brillouin zone of Fig. 5(a-b) in the phonon dispersion curves strongly implies that XVH₃ with (X=Li, K) hydrides dynamically stable [51].

3.5. Thermoelectric Properties

The world is now dealing with an energy crisis. Thermoelectric materials, which convert waste heat into electrical energy, are reported as eco-friendly, intelligent, and clean solutions to address the energy crisis[1]. Different thermoelectric properties are calculated as a function of $(\mu - \epsilon_F)$ at different temperatures, including the Seebeck coefficient (S), electrical conductivity σ , electronic thermal conductivity (κ_e), power factor ($\frac{S^2\sigma}{T}$) [1]. The outcomes, which guarantee our compositions' potential for such applications, are displayed in Fig. 6 and 7. When a temperature gradient is introduced between two junctions, a phenomenon known as see beck coefficients is produced, which results in voltage. The Seebeck coefficient is displayed in Fig. 6a and

7a for our compositions XVH₃ (X = K, Li). Plots show that at temperatures of 700 K and 300 K, respectively, the highest value of the Seebeck coefficient is $S \sim 0.0015 \text{ VK}^{-1}$ for both KVH₃ and LiVH₃ and no significant change is observed in its value with variation in temperature. The electrical conductivity variation for XVH₃ (X = K, Li) as a function of chemical potential is shown in Fig. 6b and 7b. The materials' thermoelectric qualities are closely correlated with their electrical conductivity. Electrical conductivity, or the passage of electrons from high-temperature areas to low-temperature areas, is what produces current. At a temperature of 100K, the highest values of $\sigma \sim 1.3 \times 10^{21} \text{ } \Omega^{-1} \text{ m}^{-1} \text{ s}^{-1}$ and $1.5 \times 10^{21} \text{ } \Omega^{-1} \text{ m}^{-1} \text{ s}^{-1}$, respectively, are found for these compositions, XVH₃ (X = K, Li). There are no appreciable variations in conductivity with rise in temperature. Furthermore, as shown by Fig. 6b and 7b, the equivalent value of electrical conductivity is also changing as the chemical potential increases. Thermal conductivity is the ability of a material to transfer heat which is a result of electron mobility and lattice vibrations. Fig. 6c and 7c, which fluctuate according to chemical potential at various temperature ranges, depict the thermal conductivity. The thermal conductivity peak values for XVH₃ (X = K, Li) at 900 K were around $1.2 \times 10^{16} \text{ W m}^{-1} \text{ K}^{-1} \text{ s}^{-1}$ and $1075 \times 10^{16} \text{ W m}^{-1} \text{ K}^{-1} \text{ s}^{-1}$, respectively. The correlation between temperature and thermal conductivity makes perovskite ideal for high temperature thermoelectric applications due to their close compatibility. The partial efficiency

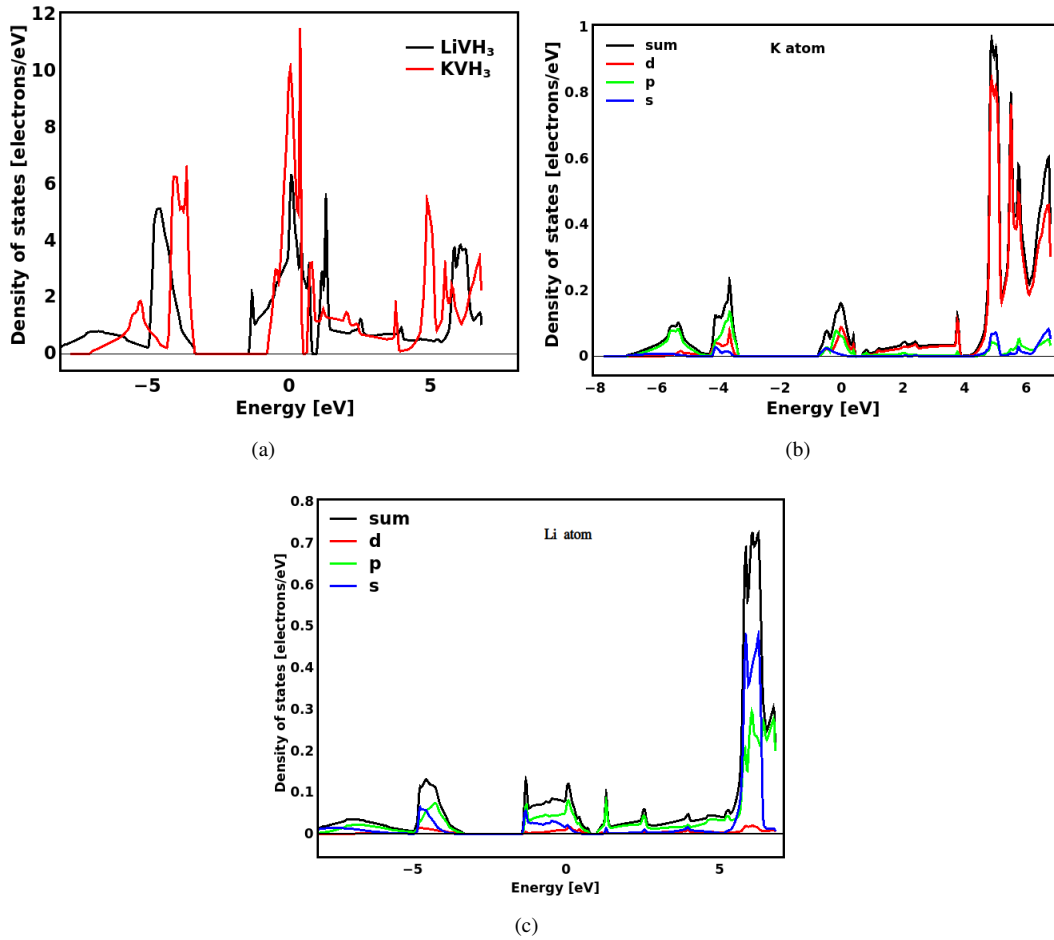


Figure 4: [DOS/PDOS for XVH₃ (X=K, Li) [a] TDOS [b] K atom PDOS [c] Li atom PDOS

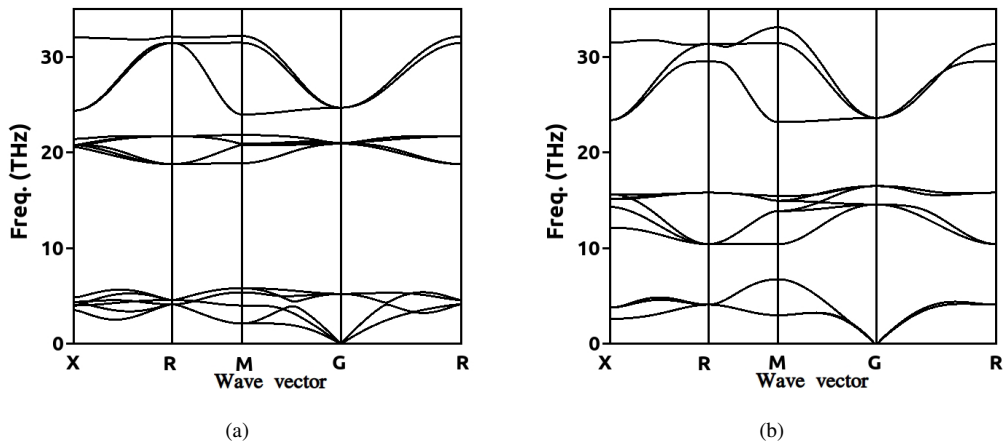


Figure 5: The phonon dispersion curves for [a] KVH₃ [b] LiVH₃

of a thermoelectric device is commonly determined by its power factor (PF). Figures 6d and 7d display the (PF) for compositions XVH₃(X = K, Li) as a function of chemical potential at different temperature ranges. The PF peaks at 100 K as the temperature rises. We deduced from the plots that the best values of (PF) for XVH₃ (X = K, Li) at

temperature 100K were around $5 \times 10^{12} W m^{-1} K^{-2} s^{-1}$ and $8 \times 10^{12} W m^{-1} K^{-2} s^{-1}$ respectively. The study presents a theoretical approach for hydrogen storage using thermoelectric compositions, revealing their strong thermoelectric responses and potential for green energy sources.

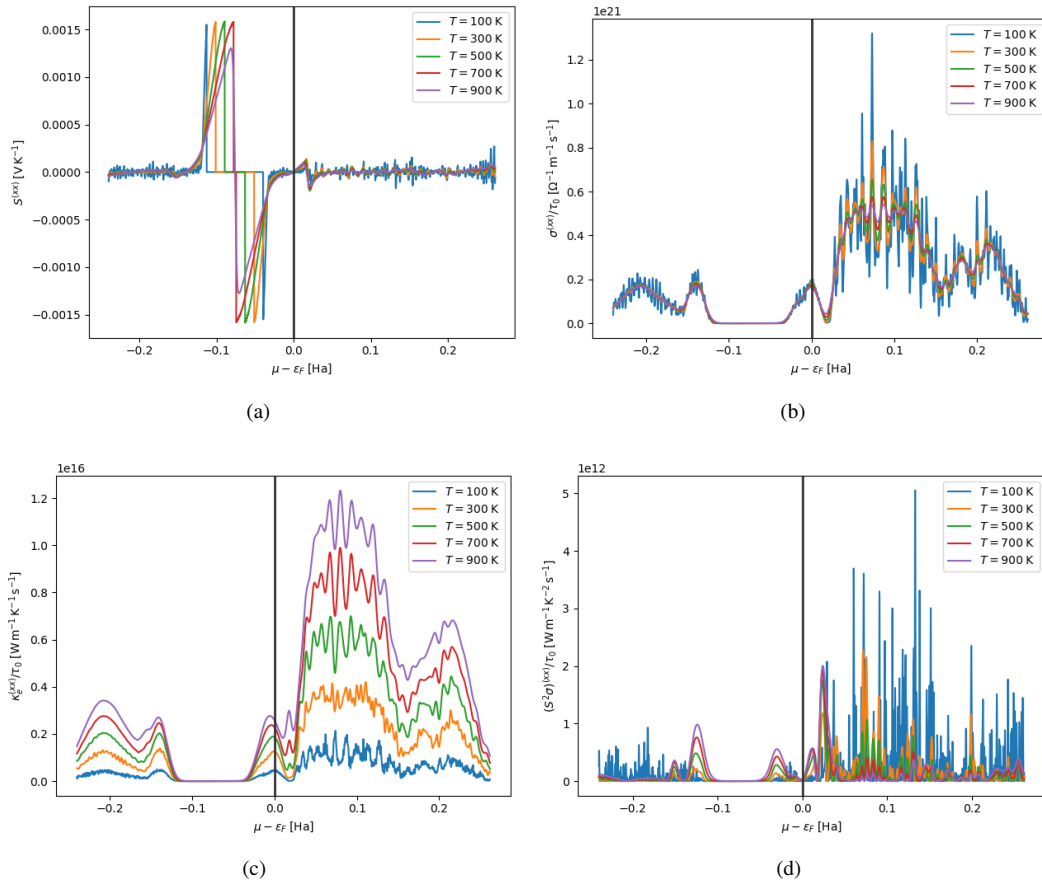


Figure 6: [a] Seebeck coefficient (S), [b] Electrical Conductivity (σ), [c] Electronic thermal conductivity (κ_e), [d] Power Factor ($S^2\sigma$) as a function of $(\mu - \epsilon_F)$ at different temperatures for KVH₃

3.6. Optical Properties

In general, the material having nonzero electronic DOS and the non-zero band gap at the fermi level is known to show the metallic character and is characterized via the electronic dynamics measurements (energy transport) along the field direction under some applied bias through a parameter called as longitudinal conductivity. On the other hand the optical conductivity originates from the interaction of material with electromagnetic radiations which have the field in transverse direction to the energy transportation. Thus, there is always possibility of getting results different than the intuitive ones. This imputed us to explore the dielectric and optical properties even after we have observed the metallic character in electronic band structure and DOS of studied compositions. These interesting and intriguing observations could be helpful for researchers exploring materials for specific frequency dependent applications such as wavefront engineering, electromagnetic tunnelling, electromagnetic cloaking etc. This section primarily focuses on the optical characteristics of materials to comprehend their interaction with electromagnetic photons [52]. The study aims to evaluate the suitability of hydroxide perovskite materials for optoelectronic applications, particularly hydrogen storage, by analyzing optical parameters based on radiation frequency. The absorption

coefficient, $\alpha(\omega)$, is a crucial factor that determines the distance light can travel through a material, influenced by the incoming light's wavelength. High absorption coefficients of materials absorb light photons more quickly, thereby stimulating the electrons in their conduction band. Fig. 8 (a) displays our calculated energy-dependent absorption coefficients for hydride perovskites, namely XVH₃ (X = Li, K). Remarkably, a notable rise in the absorption rate of LiVH₃ is observed with increasing incident radiation frequency. The maximum absorption coefficient values for XVH₃ (X = Li, K), near the infrared region are 2×10^5 and 1.7×10^5 respectively, based on the presented graphs. A material surfaces ability to reflect incoming radiation is measured by a property called reflectivity. We investigated the frequency-dependent reflectivity $R(\omega)$ of hydride perovskites and plotted graphs are shown in Figure 8(b). The peak reflectivity values for XVH₃ (X = Li, K) are 0.65 and 0.45 in the 12 to 14 eV range. The reflectance decreased rapidly as the frequency increased in the high-frequency band. The amount of energy lost by scattering or dispersion during an electron's transition is expressed by the energy loss function $L(\omega)$. The correlation is based on the scattering probabilities occurring during inner shell transitions. The optical loss function of hydride perovskites, XVH₃, is plotted against the incident

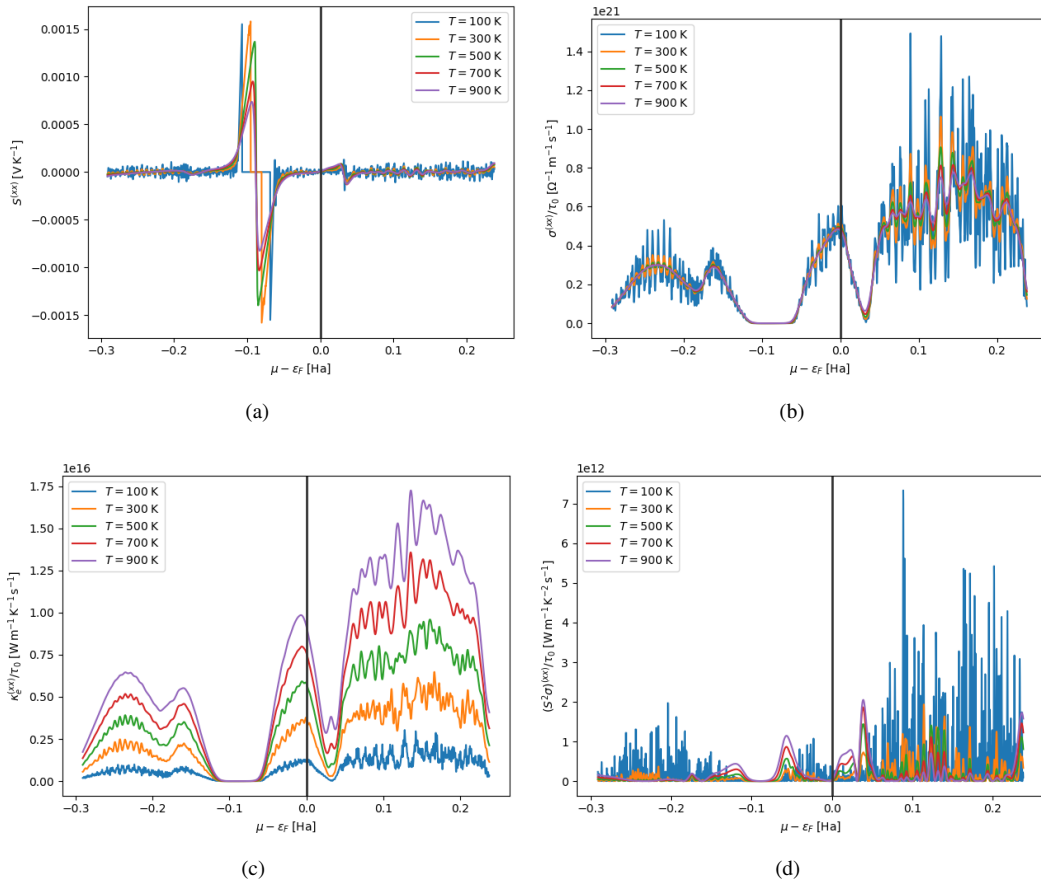


Figure 7: [a] Seebeck coefficient (S), [b] Electrical Conductivity (σ), [c] Electronic thermal conductivity (κ_e), [d] Power Factor ($S^2\sigma$) as a function of $(\mu - \epsilon_F)$ at different temperatures for LiVH₃

photon energy in Fig. 8(c). This plot exhibits a peak optical loss values of 0.9 and 1.5 at a photon energy of 2.5 and 1.9 eV for XVH₃ (X = Li, K). Plasmon emission is most likely to blame for the abrupt drop in Loss function[52] that was seen at high frequencies for all of the hydride perovskites compositions under study. It is also important to note that LiVH₃ has lesser values of loss function at high photon energy compared to KVH₃. Hence, LiVH₃ could be potential candidate for high frequency optical applications. A recent study employed optical conductivity $\sigma(\omega)$ to investigate how incident radiation interacts with the surface of XVH₃ (X = Li, K)hydride perovskites to break bonds and cause conduction through the photoelectric effect. The conductivity of hydride perovskites XVH₃ (X = Li, K) as a function of frequency is plotted against the incident photon energy, which ranges from 0 to 14 eV, as shown in Figure 8(d). LiVH₃ demonstrated the highest conductivity value, reaching 27 (1/fs) at a photon energy of 0.2 eV. The optical examination of the investigated compounds indicates that LiVH₃ is a promising material for hydrogen storage due to its high photon conductivity at low energy.

3.7. Mechanical Properties

To explore the characteristics of these compositions under high hydrostatic pressure we have calculated and reported the elastic constants as obtained using the model implemented in IRelast package integrated with Wien2k[53] for compressive force (pressure) of 5GPa and 10 GPa. These constants are calculated at a given pressure by computing the stress tensor components for tiny deformation and applying energy, in line with a lattice deformation that maintained volume [54] to provide useful information about a compound's toughness and stability. These could be experimentally obtained using Diamond Anvil Cell [55]. The strain-dependent matrix of second-order elastic constants (C_{ij}), equilibrium volume, and crystal energy are some of the variables that affect a lattice's elastic behavior. A symmetric 6X6 stiffness matrix with 21 independent components represents the material's response to applied stresses in accordance with Hooke's law. Table 2 provides information on the key elastic constants for the cubic perovskites XVH₃ (X = K, Li) i. e. C_{11} , C_{22} , and C_{44} [56]. The mechanical and elastic properties of individual perovskites compositions are largely determined by these components. The Born stability criteria, commonly known as the mechanical stability conditions, must be met by a compound having a mechanically and

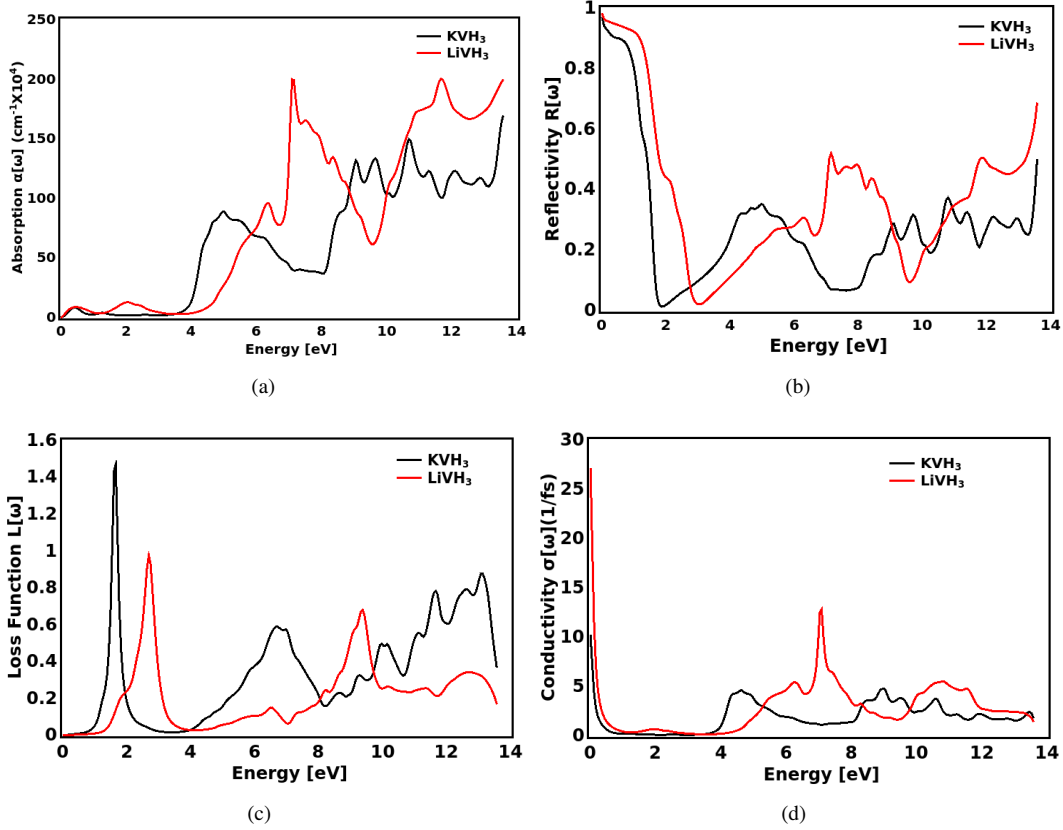


Figure 8: optical properties for XVH₃(X=Li,K) perovskite type hydrides [a] Absorption, [b] Reflectivity, [c] Loss function, [d] Conductivity

elastically stable structure. These criteria are $C_{11} > 0, C_{44} > 0, (C_{11}-C_{12}) > 0, (C_{11}+2C_{12}) > 0$ [57]. Table 2 presents three unique constants that meet the Born stability requirements, signifying the mechanical stability of every perovskite compound under investigation. Cauchy's pressure is calculated by the following equation given as

$$CP = (c_{12} - c_{44}) \quad (8)$$

B is computed as by using the V.R.H. technique:

$$B = \frac{1}{3} [c_{11} + 2c_{12}] = \frac{1}{3} \frac{1}{(s_{11} + 2s_{12})} = B_V = B_R \quad (9)$$

where

$$s_{11} = \frac{c_{11} + c_{12}}{c}; s_{12} = \frac{-c_{12}}{c}; \quad (10)$$

and

$$c = (c_{11} - c_{12})(c_{11} + 2c_{12}); s_{44} = \frac{1}{c_{44}} \quad (11)$$

Also

$$B = \frac{B_V + B_R}{2} \quad (12)$$

The following relation is used to determine Young's relation as

$$E = \frac{9GB}{3B + G} \quad (13)$$

Shear modulus is computed using the following relation as

$$G = \frac{G_R + G_V}{2} \quad (14)$$

where G_R and G_V are

$$G_V = \frac{1}{5}(c_{11} - c_{12} + 3c_{44}) \quad (15)$$

and

$$G_R = 5 \left[\frac{(c_{11} - c_{12})c_{44}}{3(c_{11} - c_{12}) + 4c_{44}} \right] \quad (16)$$

Poisson's ratio (ν) are determined using the elastic constants given by

$$k = \frac{B}{G}; G = \frac{c_{11} - c_{12} + 3c_{44}}{5} \quad (17)$$

and

$$\nu = \frac{c_{12}}{c_{11} + c_{12}} \quad (18)$$

The shear modulus (G) and Poisson's ratio (ν) are used to calculate the Young's modulus given as

$$E = 2G(1 + \nu) \quad (19)$$

Table 2

Elastic constants (C_{ij}), Bulk, Shear and Young Modulus (B_V , B_R , B , G_V , G_R , G and E_V , E_R , E in GPa), Reuss and Hill Poisson's coefficient (ν_V , ν_R in GPa), Kleinman's parameter (ζ), Ranganathan and Kube Anisotropy Index (A_u , A_k), Transverse, Longitudinal and Average wave velocity (V_t , V_l and V_a in m/s), Debye Temperature (θ_D in K), Pugh's Ratio (k), Chen and Tian Vickers hardness (H^{Cv} , H^{Tv} in GPa), Lamé's first and second parameter (λ , μ in GPa) of XVH₃ (X=Li,K) perovskites under external stress of 5 and 10 GPa.

Parameters	5 GPa		10 GPa	
	LiVH ₃	KVH ₃	LiVH ₃	KVH ₃
C_{11}	185.995	113.395	215.638	36.460
C_{12}	46.602	65.820	52.392	93.592
$C_{11}-C_{12}$	139.393	163.246	15.174	57.132
$C_{11}+2C_{12}$	279.199	225.037	320.424	223.645
C_{44}	45.824	61.112	51.297	66.685
$CP = C_{12}-C_{44}$	0.778	4.708	1.095	26.907
B_V	93.066	75.012	106.807	74.548
B_R	93.066	75.012	106.807	74.548
B	93.066	75.012	106.807	74.548
G_V	55.373	48.182	63.427	28.585
G_R	53.099	42.171	60.251	9.015
G	54.236	45.177	61.839	55.279
E_V	138.626	119.056	158.840	25.376
E_R	133.842	106.547	152.145	24.857
E	136.242	112.871	155.506	123.765
ν_V	0.252	0.235	0.252	0.330
ν_R	0.260	0.263	0.263	13.066
ν	0.256	0.249	0.257	1.430
ζ	0.462	0.821	0.452	11.541
A_u	0.214	0.713	0.264	0.345
A_k	0.094	0.298	0.115	0.326
V_t	4565.635	3909.246	4769.651	3542.125
V_l	7972.604	6763.947	8344.175	5645.832
V_a	5072.309	4339.607	5299.799	4235.564
θ_D	762.309	590.859	808.202	435.234
k	1.616	1.660	1.627	1.634
H^{Cv}	7.996	7.268	8.782	6.987
H^{Tv}	8.415	7.675	9.165	7.324
λ	56.909	44.894	65.581	43.934
μ	54.236	45.177	61.839	44.267

Ranganathan-Anisotropy Index (A_u) for cubic crystals is computed from the equation as

$$A_u = 5 \left[\frac{G_V}{G_R} - 1 \right] \quad (20)$$

Kleinman's parameter (ζ) for our compositions is computed as per equation given as

$$\zeta = \frac{c_{11} + 8c_{12}}{7c_{11} + 2c_{12}} \quad (21)$$

The value of θ_D is precisely determined for each volume V using the elastic constants by spherical average of the three components of sound velocity. It is provided as

$$\theta_D = \frac{\hbar}{k_B} 3 \sqrt{n * 6\pi^2 \sqrt{V}} \sqrt{\frac{B}{M} f_\nu} \quad (22)$$

where k_B is the Boltzmann constant, \hbar is Planck's constant, and n is the number of atoms in the primitive cell with volume V unit. A function of the Poisson ratio ν , denoted as f_ν , and M , the compound's mass, correspond to V .

$$f_\nu = 3 \sqrt{\frac{3}{2 \left[\frac{2(1+\nu)}{3(1-2\nu)} \right]^{\frac{3}{2}} + \left[\frac{(1+\nu)}{3(1-\nu)} \right]^{\frac{3}{2}}} } \quad (23)$$

Another important mechanical parameter is the degree of hardness of a material. Pugh used the formula $H_B = G \frac{b}{c}$, where b is the dislocation's Burger vector and c is a constant for all metals with the same structural composition, to create a link between the shear modulus (G) and the Brinell hardness (H_B) of pure metals. Teter discovered the

semi-empirical link between Vicker's hardness H_V and the rigidity modulus (G) as $H_V^T \sim 0.151G$. Additionally, Chen et al. provided a semi-empirical relationship between the shear modulus (G) and the squared Pugh's ratio ($k = \frac{B}{G}$), which determines Vicker's hardness.

$$H^{C_V} = 2(k^{-2}G)^{0.585} - 3 \quad (24)$$

and the same has been used to compute the values as listed in Table 2. The compositions' transverse (V_t) and longitudinal (V_l) elastic wave velocities are also calculated using the relations listed as

$$V_t = \sqrt{\frac{3B + 4G}{\rho}}; V_l = \sqrt{\frac{G}{\rho}} \quad (25)$$

where ρ represents the mass density of the composition. All mechanical properties of these compositions have been computed using equations (8-25) and are listed in table 2. Bulk modulus measures volume change under hydrostatic pressure, while shear modulus measures resistance to shape change while maintaining volume. A material's stiffness is indicated by its Young's modulus, sometimes referred to as its modulus of elasticity, which is the ratio of tensile stress to tensile strain. In summary, a stiffer material exhibits a greater Young's modulus value. The bulk, shear, and Young's moduli of LiVH₃ are found to be higher compared to KVH₃ at higher pressure hence as the table demonstrates. $\frac{B}{G}$ values can be used to identify a compound's ductility or brittleness; a ratio of less than 1.75 indicates brittleness, whereas a ratio of more than 1.75 indicates ductility [58]. The examined compositions are feably brittle in character, according to the listed values of k shown in Table 2. Crystal anisotropy influences features such as phonon modes, plastic deformation, and crack behavior, and is crucial for many technological applications. Understanding the elastic anisotropy of materials is essential to understanding these effects. The degree of anisotropy in the bonding between atoms within distinct planes can be measured using shear anisotropic factors like Ranganathan and Kube Anisotropy Index (A_u, A_k). Three factors can influence a material's behavior in different crystal orientations. As reported in table 2 all these compositions do not have value equals to one which means that they possess anisotropic behavior.

3.8. Thermodynamic Properties

The Gibbs2 code [48] has been used to estimate the thermodynamical properties of XVH₃ (X = Li, K), including thermal expansion, specific heat, volume, θ_D and entropy, as well as how these properties change with temperature (T) and pressure (P). We looked at these characteristics in the range of 0–600 K and pressure ranges from 0 to 10 GPa. The heat capacity (C_v) provides information on lattice vibration and assesses molecular mobility at a constant volume. From Figure 9(a) shows the variation of (C_v) with temperature at constant pressure. According to Dulong Petit's law (C_v) rises with an increase in temperature and become saturated at elevated temperatures. The degree of a system's disorder is measured by its entropy (S). Figure 9(b) shows the variation

of Entropy with temperature at constant pressure. There is an increase in entropy with rise in temperature. Also when the pressure is increased the degree of disorder reduces. The variation of thermal expansion coefficient (α) varies with temperature and pressure, as shown in Fig. 9(c). Due to lattice compression, the pressure variation decreases with rising temperature, while the temperature variation shows the reverse tendency. The volume increases with respect to temperature but sharply decreases with respect to pressure, as shown in Fig. 10(a) which shows that these compositions are susceptible to both pressure and temperature. The elastic constant, heat capacity, melting point, and other solid-state physical properties are connected to the Debye temperature by the QHA Debye model [43]. Figure 10(b) shows the dependency of θ_D upon pressure and temperature. At 0K and 0 GPa the computed value of θ_D is 500 K. As the temperature rises and the external pressure remained constant, the θ_D dropped. Furthermore, we observed that the θ_D increases with increasing pressure at a constant temperature. The heat capacity at stable pressure (C_p) increases monotonically with temperature. Over a range of pressure values, this pattern holds consistency as shown in Figure 10(c).

4. Conclusion

Using the DFT-based WIEN2k code, the structural, electronic, mechanical thermoelectric and thermodynamic characteristics of the Vanadium-based perovskites XVH₃ (X = Li, K) are investigated. According to the structural investigations, all compositions in space group $Pm - 3m$ [no. 221] have a stable cubic structure. They are metallic in nature, as shown by plots of the energy band gap and the density of states. Notably, the FP-LAPW approach gives us an enthalpy of formation as -248.86 kJ/mol.H₂ and -457.27 kJ/mol.H₂ for XVH₃ (X = Li, K) perovskites, which indicates these perovskites are thermodynamically stable. Furthermore, the enhanced high temperature hydrogen storage cyclability of these compositions is indicated by the high decomposition temperatures. The compositions under investigation have promising hydrogen storage potential, as demonstrated by their respective gravimetric hydrogen storage capacities of 3.25%, and 4.97% for XVH₃ (X = Li, K). Furthermore, the mechanical stability of these materials is supported by the Born stability criterion. They also showed strong thermoelectric responses, which made them suitable materials for use in thermoelectric devices as alternative green energy sources in addition to their potential for storing hydrogen.

5. Declaration of Competing Interest

The authors have no conflict of interest for the work reported in this manuscript.

CRediT authorship contribution statement

Anupam: Software, Workstation, Data generation. **Shyam Lal Gupta:** Conceptualization, Methodology, Data curation, Writing - original draft Writing - review and editing.

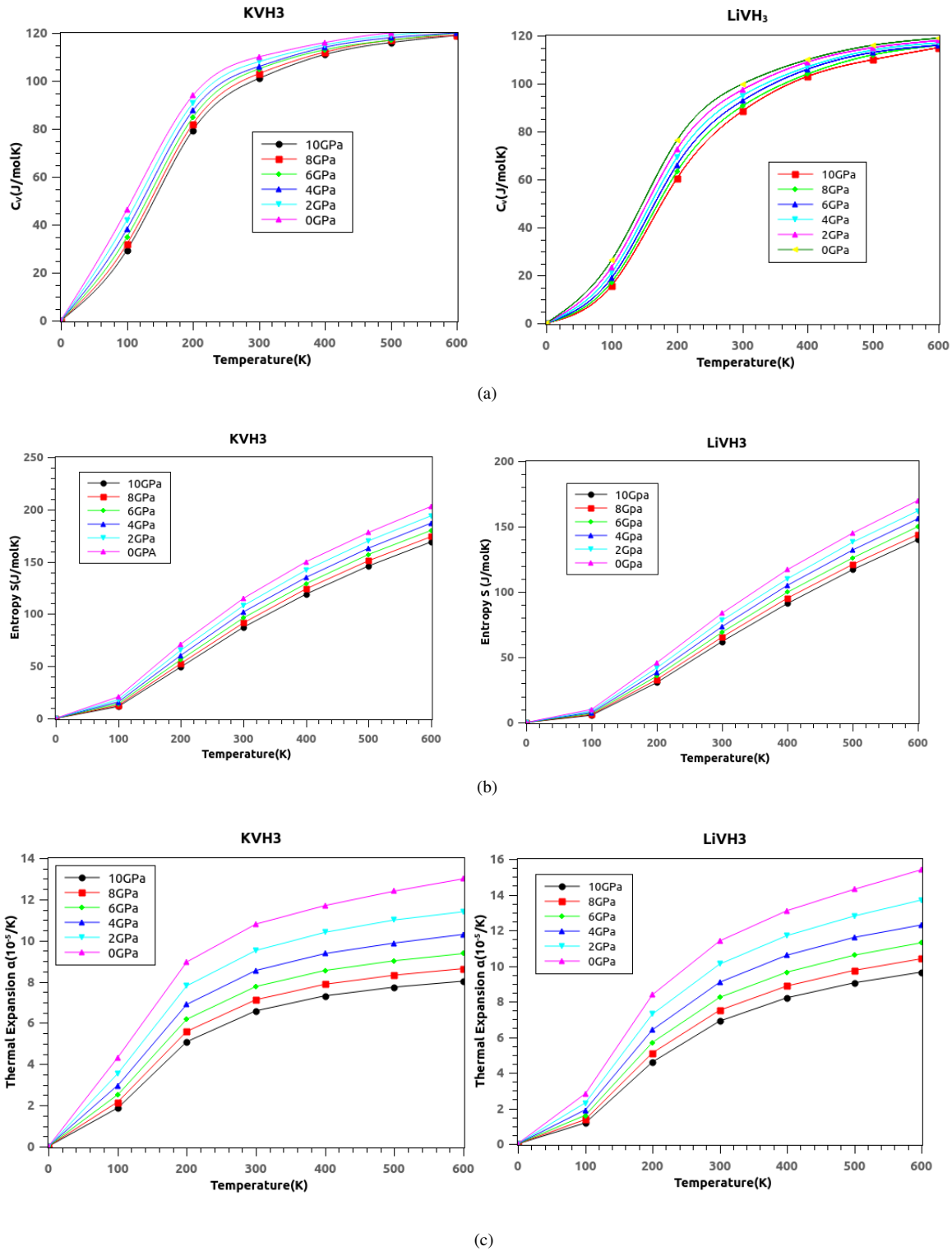


Figure 9: Variation of C_v , Entropy and Thermal expansion with temperature and pressure for XVH_3 (X=Li,K) perovskites

Sumit Kumar: Software, Workstation, Data generation.
Ashwani Kumar: Software, Workstation, Data generation.
Sanjay Panwar: Software, Workstation, Data generation.
Diwaker: Conceptualization, Methodology, Data curation, Writing - original draft Writing - review and editing.

References

- [1] Anupam, S. L. Gupta, S. Kumar, S. Panwar, Diwaker, Ab initio studies of newly proposed zirconium based novel combinations of hydride perovskites $ZrXH_3$ (X = Zn, Cd) as hydrogen storage applications, International Journal of Hydrogen Energy 55 (2024) 1465–1475.

XVH₃ (X = Li, K) as Hydrogen Storage Applications

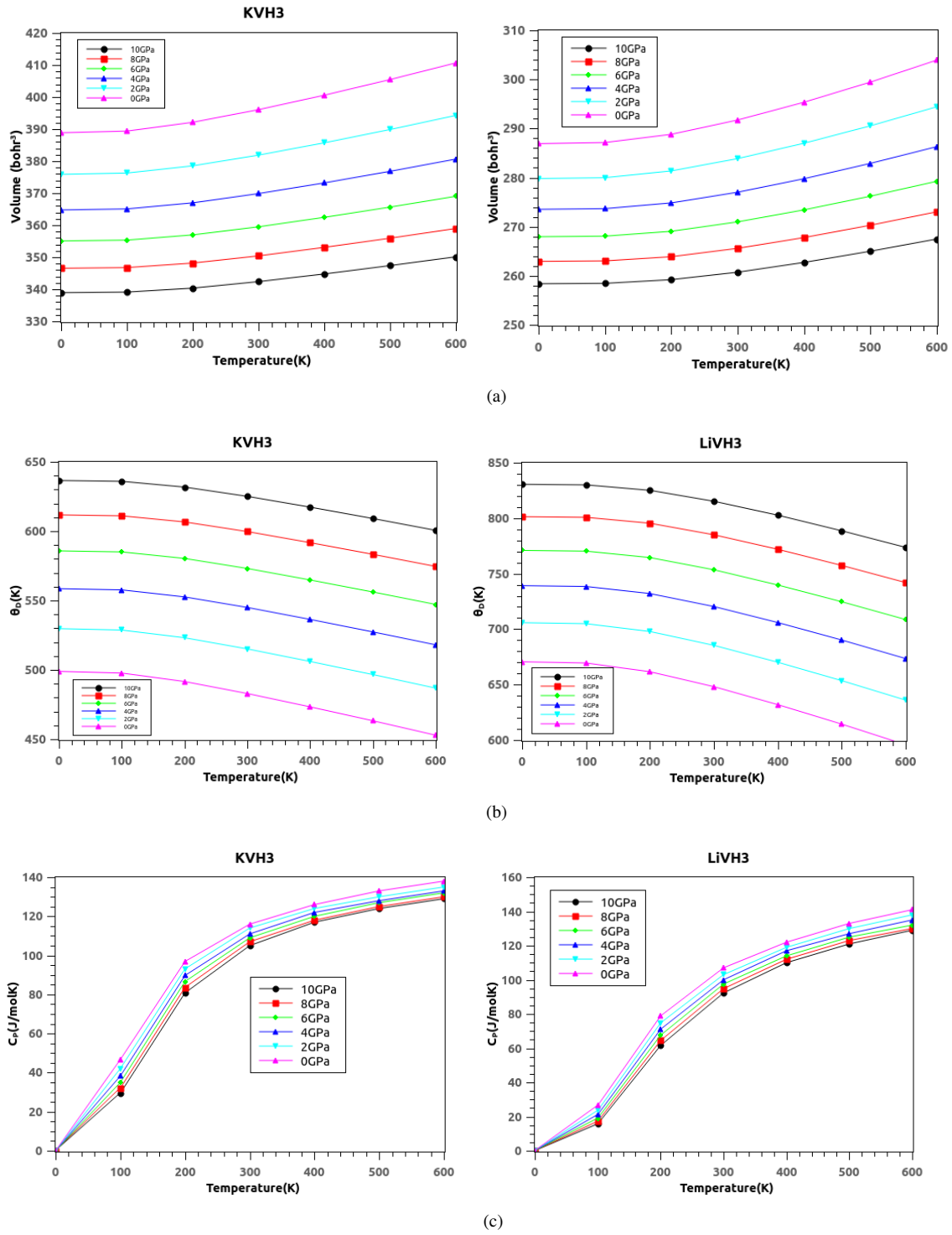


Figure 10: Variation of Volume, Debye temperature and C_p with temperature and pressure for XVH_3 ($X=Li, K$) perovskites

- [2] S. Al, N. Cavdar, N. Arikani, Computational evaluation of comprehensive properties of MgX_3H_8 ($X = Sc, Ti$ and Zr) as effective solid state hydrogen storage materials, *Journal of Energy Storage* 80 (2024) 110402.
- [3] M. A. Ullah, K. N. Riaz, M. Rizwan, Computational evaluation of $KMgO_{3-x}H_x$ as an efficient hydrogen storage material, *Journal of Energy Storage* 70 (2023) 108030.
- [4] A. Mera, M. A. Rehman, First-principles investigation for the hydrogen storage properties of $AeSiH_3$ ($Ae = Li, K, Na$ and Mg) perovskite-type hydrides, *International Journal of Hydrogen Energy* 50 (2024) 1435–1447.
- [5] B. Ahmed, M. B. Tahir, A. Ali, M. Sagir, First-principles screening of structural, electronic, optical and elastic properties of cu -based hydrides-perovskites $XCuH_3$ ($X=Ca$ and Sr) for hydrogen storage applications, *International Journal of Hydrogen Energy* 54 (2024)

- 1001–1007.
- [6] I. J. Mbonu, H. Louis, U. G. Chukwu, E. C. Agwamba, S. Ghotekar, A. S. Adeyinka, Effects of metals (X = Be, Mg, Ca) encapsulation on the structural, electronic, phonon and hydrogen storage properties of KXCl₃ halide perovskites: Perspective from density functional theory, *International Journal of Hydrogen Energy* 50 (2024) 337–351.
 - [7] R. Song, Y. Chen, S. Chen, N. Xu, W. Zhang, First-principles to explore the hydrogen storage properties of XPtH₃ (X=Li, Na, K and Rb) perovskite type hydrides, *International Journal of Hydrogen Energy* 57 (2024) 949–957.
 - [8] W. Azeem, M. K. Shahzad, Y. H. Wong, M. B. Tahir, Ab-initio calculations for the study of the hydrogen storage properties of CsXH₃ (X= Co, Zn) perovskite-type hydrides, *International Journal of Hydrogen Energy* 50 (2024) 305–313.
 - [9] N. Xu, Y. Chen, S. Chen, S. Li, W. Zhang, First-principles investigation for the hydrogen storage properties of XTiH₃ (X=K, Rb and Cs) perovskite type hydrides, *International Journal of Hydrogen Energy* 50 (2024) 114–122.
 - [10] B. Ahmed, M. B. Tahir, A. Ali, M. Sagir, Dft insights on structural, electronic, optical and mechanical properties of double perovskites X₂FeH₆ (X = Ca and Sr) for hydrogen-storage applications, *International Journal of Hydrogen Energy* 50 (2024) 316–323.
 - [11] A. Mera, M. A. Rehman, First-principles investigation for the hydrogen storage properties of AeSiH₃ (Ae = Li, K, Na and Mg) perovskite-type hydrides, *International Journal of Hydrogen Energy* 50 (2024) 1435–1447.
 - [12] S. Cheng, X. Cheng, M. H. Tahir, Z. Wang, J. Zhang, Synthesis of rice husk activated carbon by fermentation osmotic activation method for hydrogen storage at room temperature, *International Journal of Hydrogen Energy* 62 (2024) 443–450.
 - [13] X. Xu, Y. Dong, Q. Hu, N. Si, C. Zhang, Electrochemical hydrogen storage materials: State-of-the-art and future perspectives, *Energy & Fuels* 38 (2024) 7579–7613.
 - [14] M. A. Rehman, J. Fatima, Z. U. Rehman, S. Y. Alomar, M. Sohiab, A. Hamad, The dft study of the structural, hydrogen, electronic, mechanical, thermal, and optical properties of KXH₃ (X = Ca, Sc, Ti and Ni) perovskite-type hydrides, *Structural Chemistry* (2024) 1572–9001.
 - [15] Z. U. Rehman, M. A. Rehman, B. Rehman, S. Sikiru, S. Qureshi, E. M. Ali, M. Awais, M. Amjad, I. Iqbal, A. Rafique, S. Bibi, Ab initio insight into the physical properties of MgXH₃ (X = Co, Cu and Ni) lead free perovskite for hydrogen storage applications, *Environmental Science and Pollution Research* (2023) 113889–113902.
 - [16] S. Bahhar, A. Tahiri, A. Jabar, M. Louzazni, M. Idiri, H. Bioud, Computational assessment of MgXH₃ (X = Al, Sc and Zr) hydrides materials for hydrogen storage applications, *International Journal of Hydrogen Energy* 58 (2024) 259–267.
 - [17] M. U. Ghani, M. Sagir, M. B. Tahir, S. Ullah, M. A. Assiri, An extensive study of structural, electronic, elastic, mechanical and optical properties of XCdH₃ (X=K, Rb) for hydrogen storage applications: First-principles approach, *International Journal of Hydrogen Energy* 55 (2024) 1265–1272.
 - [18] A. Siddique, A. Khalil, B. S. Almutairi, M. B. Tahir, M. Sagir, Z. Ullah, A. Hannan, H. E. Ali, H. Alrobei, M. Alzaid, Structures and hydrogen storage properties of AeVH₃ (Ae = Be, Mg, Ca and Sr) perovskite hydrides by dft calculations, *International Journal of Hydrogen Energy* 48 (2023) 24401–24411.
 - [19] M. Rkhis, S. Laasri, S. Touhtouh, E. K. Hlil, M. Bououdina, R. Ahuja, K. Zaidat, S. Obbade, A. Hajjaji, Engineering the hydrogen storage properties of the perovskite hydride ZrNiH₃ by uniaxial/biaxial strain, *International Journal of Hydrogen Energy* 47 (2022) 3022–3032.
 - [20] H. H. Raza, G. Murtaza, U. e Hani, N. Muhammad, S. M. Ramay, First-principle investigation of XSrH₃ (X = K and Rb) perovskite-type hydrides for hydrogen storage, *Int J Quantum Chem* 120 (2020) e26419.
 - [21] R. M. A. Khalil, M. I. Hussain, F. Hussain, A. M. Rana, G. Murtaza, M. Shakeel, H. M. Asif Javed, Structural, vibrational, mechanical, and optoelectronic properties of LiBH₄ for hydrogen storage and optoelectronic devices: First-principles study, *Int J Quantum Chem* 121 (2021) e26444.
 - [22] S. Al, M. Yortanlı, E. Mete, Lithium metal hydrides (Li₂CaH₄ and (Li₂SrH₄ for hydrogen storage; mechanical, electronic and optical properties, *International Journal of Hydrogen Energy* 45 (2020) 18782–18788.
 - [23] J. Bellosta von Colbe, J.-R. Ares, J. Barale, M. Baricco, C. Buckley, G. Capurso, N. Gallandat, D. M. Grant, M. N. Guzik, I. Jacob, E. H. Jensen, T. Jensen, J. Jepsen, T. Klassen, M. V. Lototsky, K. Manickam, A. Montone, J. Puszkiel, S. Sartori, D. A. Sheppard, A. Stuart, G. Walker, C. J. Webb, H. Yang, V. Yartys, A. Züttel, M. Dornheim, Application of hydrides in hydrogen storage and compression: Achievements, outlook and perspectives, *International Journal of Hydrogen Energy* 44 (2019) 7780–7808.
 - [24] Padhee, S. P., Roy, A., Pati, S., Mechanistic insights into efficient reversible hydrogen storage in ferrotitanium, *International Journal of Hydrogen Energy* 46 (2021) 906–921.
 - [25] S. P. Padhee, A. Roy, S. Pati, Role of Mn-substitution towards the enhanced hydrogen storage performance in FeTi, *International Journal of Hydrogen Energy* 47 (2022) 9357–9371.
 - [26] Chattaraj, D., Dash, S., Majumder, C., Structural, electronic, elastic, vibrational and thermodynamic properties of ZrNi and ZrNiH₃: A comprehensive study through first principles approach, *International Journal of Hydrogen Energy* 41 (2016) 20250–20260.
 - [27] Zapatero, P. A., Herrero, A., Lebon, A., Gallego, L. J., Vega, A., Ab initio study of lithium decoration of popgraphene and hydrogen storage capacity of the hybrid nanostructure, *International Journal of Hydrogen Energy* 46 (2021) 15724–15737.
 - [28] Abdellaoui, M., Lakhal, M., Benzidi, H., Mounkachi, O., Benyoussef, A., Kenz, A. E., Loulidi, M., The hydrogen storage properties of Mg-intermetallic-hydrides by ab initio calculations and kinetic monte carlo simulations, *International Journal of Hydrogen Energy* 45 (2020) 11158–11166.
 - [29] T. Sato, D. Noréus, H. Takeshita, U. Häussermann, Hydrides with the perovskite structure: General bonding and stability considerations and the new representative CaNiH₃, *Journal of Solid State Chemistry* 178 (2005) 3381–3388.
 - [30] L. Klebanoff, J. Keller, 5 years of hydrogen storage research in the U.S. doe metal hydride center of excellence (MHCoE), *International Journal of Hydrogen Energy* 38 (2013) 4533–4576.
 - [31] D. Broom, C. Webb, G. Fanourgakis, G. Froudakis, P. Trikalitis, M. Hirscher, Concepts for improving hydrogen storage in nanoporous materials, *International Journal of Hydrogen Energy* 44 (2019) 7768–7779.
 - [32] A. Züttel, Materials for hydrogen storage, *Materials Today* 6 (2003) 24–33.
 - [33] S. J. Park, M.K. Seo, Interface science and composites, *Elsevier* 18 (2011) 1–143.
 - [34] U. A. Khan, N. U. Khan, Abdullah, A. H. Alghtani, V. Tirth, S. J. Ahmed, M. Sajjad, A. Algahtani, T. Shaheed, A. Zaman, First-principles investigation on the structural, electronic, mechanical and optical properties of silver based perovskite AgXCl₃ (X= Ca, Sr), *Journal of Materials Research and Technology* 20 (2022) 3296–3305.
 - [35] G. Surucu, A. Gencer, A. Candan, H. H. Gullu, M. Isik, CaXH₃ (X = Mn, Fe, Co) perovskite-type hydrides for hydrogen storage applications, *International Journal of Energy Research* 44 (2020) 2345–2354.
 - [36] S. Razaq, G. Murtaza, R. M. A. Khalil, N. Ahmad, H. H. Raza, Ab-initio calculation of electronic, mechanical, optical and phonon properties of ZrXH₃ (X = Co, Ni and Cu): A key towards potential hydrogen storage materials, *International Journal of Modern Physics B* 36 (2022) 2250090.
 - [37] Blaha, P., Schwarz, K., Tran, F., Laskowski, R., Madsen, G. K. H., Marks, L. D., WIEN2k: An APW+lo program for calculating the properties of solids, *The Journal of Chemical Physics* 152 (2020).
 - [38] Y. Xu, B. Peng, H. Zhang, H. Shao, R. Zhang, H. Zhu, Irelast package, *Journal of Alloys and Compounds* 735 (2018) 569–579.

- [39] F. Tran, P. Blaha, Accurate band gaps of semiconductors and insulators with a semilocal exchange-correlation potential, *Phys. Rev. Lett.* 102 (2009) 226401.
- [40] P. Borlido, J. Schmidt, A. W. Huran, F. Tran, M. A. L. Marques, S. Botti, Exchange-correlation functionals for band gaps of solids: benchmark, reparametrization and machine learning, *npj Computational Materials* 6 (2020) 96.
- [41] T. Rauch, M. A. L. Marques, S. Botti, Local modified becke-johnson exchange-correlation potential for interfaces, surfaces, and two-dimensional materials, *Journal of chemical theory and computation* 16 (2020) 2654–2660.
- [42] F. Tran, J. Doumont, L. Kalantari, P. Blaha, T. Rauch, P. Borlido, S. Botti, M. A. L. Marques, A. Patra, S. Jana, P. Samal, Bandgap of two-dimensional materials: Thorough assessment of modern exchange-correlation functionals, *The Journal of Chemical Physics* 155 (2021) 104103.
- [43] A. Kumar, S. L. Gupta, V. Kumar, S. Kumar, Anupam, Diwaker, Spin-polarized dft investigations of novel KVSb half-Heusler compound for spintronic and thermodynamic applications, *Physica B: Condensed Matter* 691 (2024) 416366.
- [44] S. L. Gupta, S. Singh, S. Kumar, Anupam, S. S. Thakur, A. Kumar, S. Panwar, Diwaker, Ab-initio stability of iridium based newly proposed full and quaternary Heusler alloys, *Physica B: Condensed Matter* 674 (2024) 415539.
- [45] S. L. Gupta, S. Kumar, Anupam, S. S. Thakur, S. Panwar, Diwaker, A newly proposed full Heusler alloy Ir₂VZ (Z=Sn, In) suitable for high-temperature thermoelectric applications: A dft approach, *Modern Physics Letters B* 38 (2024) 2450030.
- [46] A. Kumar, T. Chandel, Diwaker, N. Thakur, Robust stability, half-metallic ferromagnetism and structural properties of Co₂RhSi and Co₂RuSi Heusler compounds—a first principles approach, *Materials Today: Proceedings* 66 (2022) 3292–3297. *Condensed Matter Physics (CMDAYS 2021)*.
- [47] G. K. Madsen, J. Carrete, M. J. Verstraete, Boltztrap2, a program for interpolating band structures and calculating semi-classical transport coefficients, *Computer Physics Communications* 231 (2018) 140–145.
- [48] A. O. de-la Roza, V. Luaña, Gibbs2: A new version of the quasi-harmonic model code. i. robust treatment of the static data, *Computer Physics Communications* 182 (2011) 1708–1720.
- [49] H. Li, S. Zhao, W. Zhang, H. Du, X. Yang, Y. Peng, D. Han, B. Wang, Z. Li, Efficient esterification over hierarchical Zr-beta zeolite synthesized via liquid-state ion-exchange strategy, *Fuel* 342 (2023) 127786.
- [50] A. Gencer, G. Surucu, S. Al, MgTiO₃H_x and CaTiO₃H_x perovskite compounds for hydrogen storage applications, *International Journal of Hydrogen Energy* 44 (2019) 11930–11938.
- [51] P. Zhao, J. Zhu, M. Li, G. Shao, H. Lu, H. Wang, J. He, Theoretical and experimental investigations on the phase stability and fabrication of high-entropy monoborides, *Journal of the European Ceramic Society* 43 (2023) 2320–2330.
- [52] Z. U. Rehman, M. A. Rehman, H. Chaudhry, M. Awais, Ab initio insight into the structural, vibrational, electronic, optical, magnetic, and thermal properties of lead-free perovskite Cs₃Sb₂Cl₉ for solar cell application, *Journal of Physics and Chemistry of Solids* 182 (2023) 111548.
- [53] M. Jamal, M. Bilal, I. Ahmad, S. Jalali-Asadabadi, Irelast package, *Journal of Alloys and Compounds* 735 (2018) 569–579.
- [54] J. Wang, S. Yip, S. R. Phillpot, D. Wolf, Crystal instabilities at finite strain, *Phys. Rev. Lett.* 71 (1993) 4182–4185.
- [55] V. I. Levitas, M. Kamrani, B. Feng, Tensorial stress strain fields and large elastoplasticity as well as friction in diamond anvil cell up to 400, *npj Computational Materials* 5 (2019) 94.
- [56] X. Wang, X. Li, H. Xie, T. Fan, L. Zhang, K. Li, Y. Cao, X. Yang, B. Liu, P. Bai, Effects of Al and La elements on mechanical properties of CoNiFe_{0.6}Cr_{0.6} high-entropy alloys: a first-principles study, *Journal of Materials Research and Technology* 23 (2023) 1130–1140.
- [57] M. Born, On the stability of crystal lattices. i, *Mathematical Proceedings of the Cambridge Philosophical Society* 36 (1940) 160–172.
- [58] V. V. Bannikov, I. R. Shein, A. L. Ivanovskii, Electronic structure, chemical bonding and elastic properties of the first thorium-containing nitride perovskite tathn3, *physica status solidi (RRL) – Rapid Research Letters* 1 (2007) 89–91.